Energy Storage Materials 56 (2023) 572–581

Contents lists available at ScienceDirect

Energy Storage Materials

journal homepage: www.elsevier.com/locate/ensm

Stabilizing nucleation seeds in Li metal anode via ion-selective graphene oxide interfaces

Jingjing Ma [a,b], Jinlong Yang [c], Can Wu [d], Meng Huang [c], Jiawei Zhu [a], Weihao Zeng [a], Lun Li [b], Peng Li [b], Xin Zhao [b], Fan Qiao [a], Zixin Zhang [b], Daping He [b,*], Shichun Mu [a,*]

[a] State Key Laboratory of Advanced Technology for Materials Synthesis and Processing, Wuhan University of Technology, Wuhan 430070, Hubei, China
[b] Hubei Engineering Research Center of RF-Microwave Technology and Application, Wuhan University of Technology, Wuhan 430070, China
[c] Guangdong Research Center for Interfacial Engineering of Functional Materials, College of Materials Science and Engineering, Shenzhen University, Shenzhen 518060, China
[d] Science and Technology Institute of Advanced Technology, Wuhan 430051, China

ARTICLE INFO

Keywords:
Lithium metal anode
Lithiophilic sites
Graphene oxide
Sustainable alloy sites
Ion selectivity

ABSTRACT

Inhomogeneous lithium deposition is an intractable issue that would cause the uncontrollable formation of lithium dendrites, triggering the cycle-life and safety concern of lithium-metal batteries. Constructing lithiophilic sites is considered as an effective approach to modify the lithiophobic Cu current collector. However, whether the lithiophilic site is stable or can sustainably regulate the lithium deposition in the long-term cycling still keeps unknown. Herein, we conceive a unique "sandwich" anode composed of nanoscale Zn metals uniformly confined between GO and Cu foil. In such a unique structure the middle layer of lithiophilic Zn nanoparticles as a nucleation seed facilitates the deposition of lithium to form a zinc-lithium alloy, while the GO layer at the interface not only provides a channel for the rapid transport of lithium ions, but also has strong adsorption properties with Zn to ensure the stability of the nucleation seed during long-term cycling. As a result, the GO-protected alloy composite anode has a smaller overpotential and more stable cycling than the pure alloy anode and the graphene-protected unalloyed anode. Consequently, a high Coulombic efficiency above 98% for 200 cycles at 1 mA cm^{-2} and a prolonged lifespan of symmetrical cells for 600 h at 1 mA cm^{-2} with lower polarization are achieved, which further renders the commercial $LiFePO_4$ (LFP) based full cell cathode (11.5 mg cm^{-2}) with high rate capacity of 90 mAh g^{-1} at 5 C) and high capacity retention of 81.1% at 1 C after 100 cycles. This work provides a new insight into high-efficiency Li storage by sustainable alloy sites.

1. Introduction

Currently, the energy density and lifetime of lithium-ion batteries (LIBs) are more and more difficult to meet the demand of electric devices. Metallic Li, with an ultrahigh specific capacity of 3860 mAh g^{-1} and the lowest reduction potential (-3.04 V versus standard hydrogen electrode), has been considered as an effective material to increase the energy density of Li-metal batteries (LMBs) up to 500 Wh kg^{-1} [1–3]. However, the practical application of LMBs is still hindered by the uneven deposition of Li caused by Li dendrite growth and infinite volume change, resulting in aggravated unstable solid-electrolyte interphase (SEI) layers and low Coulombic efficiency (CE). With increasing cycle times, the continuous formation of Li dendrites leads to the accumulation of "dead" Li, decreased CE, and even increased safety hazards [4–6].

To address these issues, first, the mechanism of Li stripping/plating transformation was deeply analyzed, and it was found that many parameters of host would affect Li deposition, such as the high conductivity can reduce the local current density, and uniform the Li deposition [7]. Also, the current density and external pressure are key factors in improving the accumulation of inactive Li [8], and the formation of uniform and stable SEI is crucial for battery cycle [9]. Thus numerous strategies have been developed [10,11]. A general view from the electrochemistry of Li metal deposition/dissolution is the design of lithiophilic sites [12], which is needed to modify the lithiophobic copper (Cu) current collector for improved reversibility and stability of the Li metal during charging and discharging [13,14]. Considering the important role of heterogeneous nanoseeds in tuning the Li stripping and plating behavior of Li metal anode, as proposed by Cui *et al.* [15] in their

* Corresponding authors.
E-mail addresses: hedaping@whut.edu.cn (D. He), msc@whut.edu.cn (S. Mu).

https://doi.org/10.1016/j.ensm.2023.01.045
Received 1 December 2022; Received in revised form 17 January 2023; Accepted 28 January 2023
Available online 31 January 2023

pioneering works, metal nanoparticles (NPs) (such as Au, Ag and Mg) with low overpotentials of Li nucleation have been proven preferentially nucleate and grow inside the nanospheres, effectively guiding Li deposition within carbonaceous host materials [3,15-19]. For example, single-atom metal Zn sites in carbon matrices [20] possessed higher surface energy to stabilize Li atoms, and the lower Li migration barrier energy to improve high dimensional Li deposition kinetics. Such a modification achieved a low overpotential about 12 mV and high CE up to 100%. Thus, Zn could induce Li growth, facilitating the uniform and dendrite-free deposition.

Despite the substantial progress and growing interest in heteroparticles/atoms which induce Li plating and reduce nucleation overpotentials during Li deposition by means of alloying (such as Li_xAu [15], Li_xZn [21], and Li_xAl [22]), little work has focused on the failure mechanism of the lithiophilic metal among alloys after dealloying and the persistency of the nucleation site after cycling. It has been emphasized that the sustainability of lithophilic sites plays an important role during cycling. The rapid accumulation of "dead" Li covers the lithiophilic sites and blocks the diffusion channels of Li ions to the lithiophilic sites, resulting in the gradual failure of lithophilic sites, which increases the nucleation overpotentials and induces low internal resistance under practical conditions [23]. Meanwhile, the lithiophilic site of metal-based [24] and metal-oxide-based [25,26] materials is particularly susceptible to fall off under a high cycling capacity, as their components/structures may change during this period, which is also vital but neglectful. Therefore, deciphering the evolution process of lithiophilic sites under dealloying is imperative for designing stable Li metal composite anode.

In this work, we first electrodeposit Zn metal NPs on Cu foil as lithiophilic deposition sites and investigate their structural evolution, and subsequently propose a positive role of graphene oxide (GO) in stabilizing the Zn seed for deposition-dissolution of Li metal. Both theoretical and experimental results of Li electrochemistry confirm that 1) the Zn^{2+} is easy to enter the electrolyte from the alloy during Li stripping; 2) the GO has a strong adsorption effect on Zn^{2+}, thus ensuring its stability; 3) the GO as an artificial interface with high Li-ion conductivity effectively promotes Li ion diffusion. Hence, the GO has the ability to improve Li ion conductivity and maintain the stability of Li-philic Zn layers on Li metal electrode. Consequently, under the synergy of these advantages, the half cells assembled with GO-Zn/Cu anodes exhibit stable and high average CE. And the full cells with commercial $LiFePO_4$ (LFP) electrode further show significantly enhanced cycling stability and the highest capacity retention compared with other electrodes. Moreover, it can be assembled into a flexible pouch battery, indicating its potential applications in flexible and wearable electronics.

2. Results and discussion

Theoretical calculations. First, a comprehensive computational method was carried out to understand the molecular structure, surface properties of GO, in which different chemical environments, such as

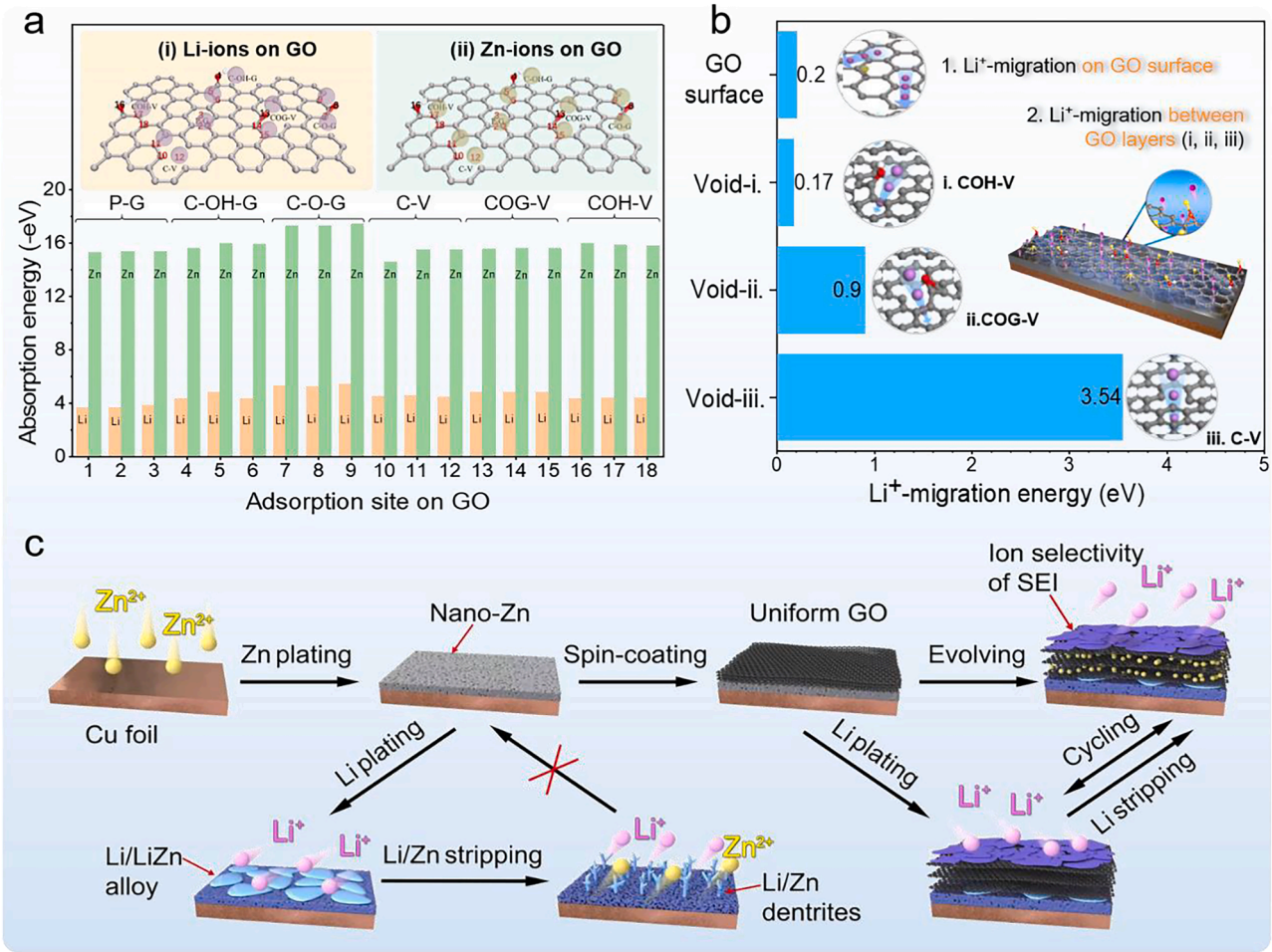

Fig. 1. (**a**) DFT calculation models and statistical chart of binding energy between Zn^{2+}, Li^+ and 18 sites of GO in P-G, C-O-G and C-OH-G groups, even in C-V, COG-V and COH-V groups. (**b**) Binding energy of Li^+ migration path and schematic diagram (inset) on the surface and layers of GO. (**c**) Design and functioning mechanism of the GO-Zn/Cu three-layer structured electrode.

pure graphene (P-G), epoxy group (C-O-G), hydroxyl (C-OH-G), pure GO with defects (C-V), GO with epoxy group and defects (COG-V), and GO with hydroxyl group and defects (COH-V) were considered [27–29]. From the binding energy of GO to different metal ions on various sites (Fig. 1a), it shows higher absorption energy between GO and Zn^{2+} than that between GO and Li^{+} on the 18 sites, indicating stronger trapping force for Zn^{2+} on GO. From the comparison of the binding energy between GO and two metal ions at each of the 18 sites the absorption energy between GO and Zn^{2+} at each site is higher than that between GO and Li^{+}, which indicates that GO has a stronger trapping power to Zn^{2+}. This anchoring effect for Zn^{2+} is beneficial for reducing the transmission of Zn^{2+} into the electrolyte, maintaining the Zn layer and thus providing stable Li storage sites.

Additionally, the migration barrier of Li-ions on the surface of GO is only 0.197 (~0.2) eV (Fig. 1b), enabling free transportation on GO surfaces. Meanwhile, the C-O-G and C-OH-G possess a strong chemical bond (M-O) for Li^{+} to functional groups, such as Li_2O, which is a well-known conductive Li^{+} component (Fig. S1 and S2) [30]. Thus, the energy barrier for Li^{+} diffusion can be decreased vertically across GO layers, and as shown in Fig. S3, the Li ions can easily migrate in the vertical direction at the defects of the graphene layer. For the defect without functional groups, the energy barrier is as high as 3.54 eV. By contrast, the COG-V and COH-V functional groups on GO contribute to much lower barriers of 0.902 and 0.17 eV, respectively, demonstrating that the defect and functional group favor Li^{+} diffusion through GO (Fig. 1b).

Material synthesis and characterizations. Inspired by the theoretical findings, we constructed a GO-Zn/Cu three-layer structure electrode as hosts for Li deposition/stripping (Detailed experiments in Supporting information). During cycling, Li^{+} ions are preferentially deposited at the lithiophilic Zn site that can reduce nucleation barriers and form Li/LiZn layers. However, the dissolution of Zn^{2+} results in the loss of the Li-philic layer during Li^{+} electrochemical stripping of Zn/Cu electrode. While the GO as a protective layer improves the sustainability of the lithophilic layer on the GO-Zn/Cu electrode. The Zn can be anchored by the GO film due to stronger binding energy than Li. In addition, Li^{+} can successfully migrate on the surface until it reaches the defect because of the low surface migration energy and formation of native SEI components. Then Li can diffuse to the next layer through the defect (Void-i, ii, iii). Meanwhile, GO is beneficial in maintaining the integrity of SEI due to its highly flexible and mechanical surface properties. Taken together, the DFT simulation results corroborate the advanced feature of GO as good interface materials for protecting anode and suppressing Li-dendrites (Fig. 1c).

The construction process of GO-Zn/Cu is illustrated in Fig. S4. Initially, pristine Zn was in-situ deposited on the rough surface of Cu foil (~11.5 μm thick) in an electrolytic cell. The time and rate of deposition were adjusted to optimize the morphology of electroplated Zn layers, and different characteristics of the samples can be obtained and presented as flakes, agglomeration and nanoparticles, respectively (Fig. S5). It is notable that the nano-Zn matrix with 3D interstices (~4.5 μm) is the optimal choice, which can provide more lithiophilic sites, reduce nucleation barriers, and then show more stable Li plating/stripping performance (Fig. S6). Then GO (~0.4 μm) modified Zn/Cu through

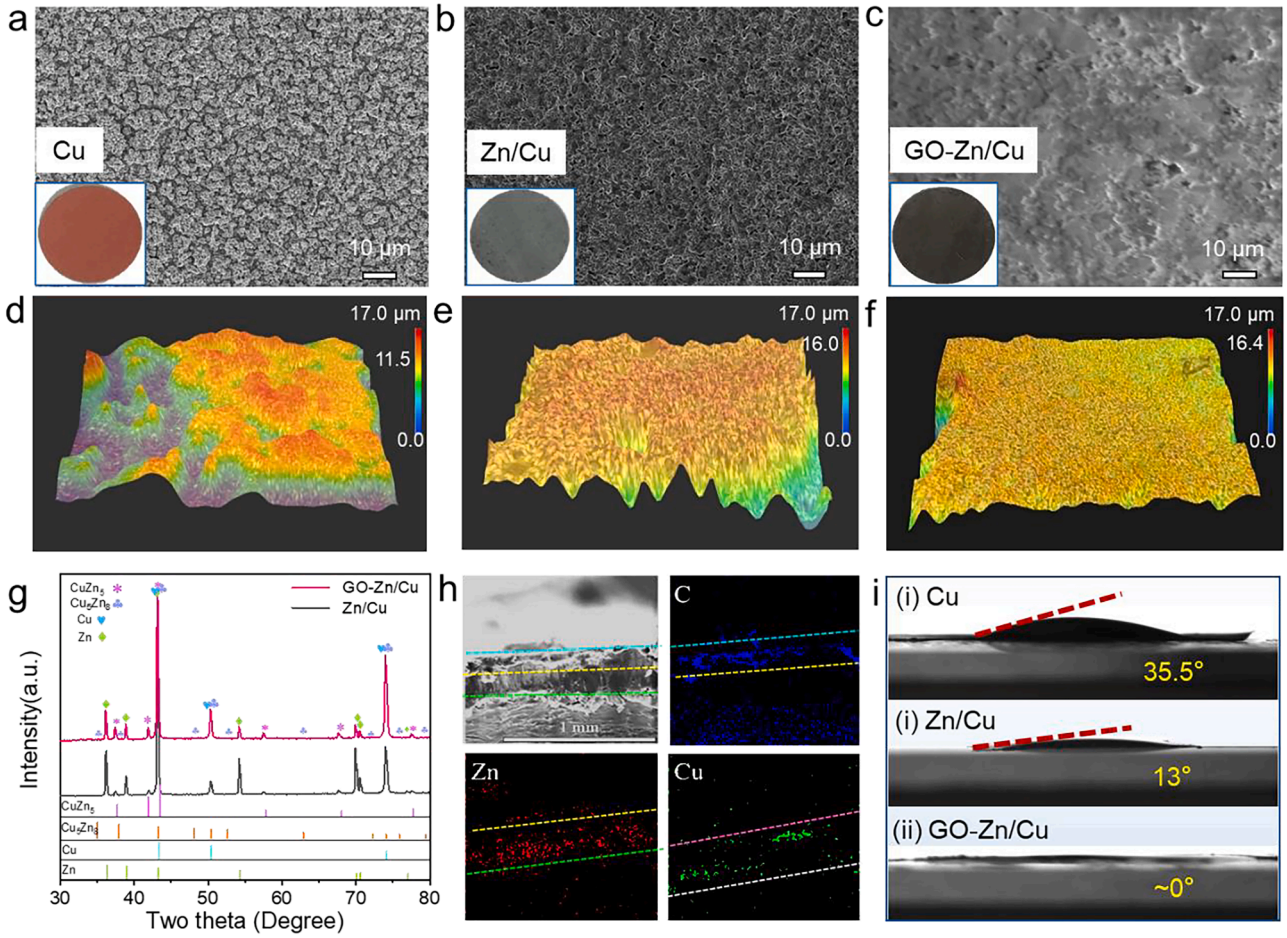

Fig. 2. Structural characterizations of various substrates. (**a-c**) SEM and digital images (inset) of GO-Zn/Cu, Zn/Cu, and pure Cu substrates, and (**d-f**) 3D maps of super depth of field of Cu, Zn/Cu, and GO-Zn/Cu. (**g**) XRD patterns of GO-Zn/Cu and Zn/Cu electrodes. (**h**) Element mappings of the GO-Zn/Cu electrode. (**i**) Contact angles of electrolyte on Cu, Zn/Cu and GO-Zn/Cu electrode.

spin-coating (GO-Zn/Cu) can prevent the loss caused by the stripping of impurity ions in the alloy anode. Scanning electron-microscopy (SEM) and corresponding digital images (inner) demonstrate the evolution of GO-Zn/Cu that the morphology changes from the rough Cu surface (Fig. 2a) to the nano-Zn structure (Fig. 2b), and finally forms smooth composite substrate (Fig. 2c). The super-high magnification lens zoom 3D microscope fields provide additional evidences to the uniform and flat construction of 3D structured anode with the two-step coating process (Fig. 2d, e, f). The flat surface of substrate facilitates uniform Li deposition. The sandwich structure constructed by graphene layers and nano-Zn provides affinity for electrodeposited Li and hence effectively promotes the chemical reaction between Li and Zn. The Li/LiZn was fabricated by contacting GO-Zn/Cu with Li. LiZn alloy was commonly used as anode material with high specific capacities. Meanwhile, the ex-situ GO protective layer of GO-Zn/Cu electrode can access easily for alkali ion diffusion via defects [31–33]. With the final modification of GO layers, the smooth morphology was obtained, which can reduce uneven Li-ion flow. Meanwhile, the XRD pattern of Zn/Cu electrode reveals the presence of CuZn alloy phases (Fig. 2g), which supplies close contact between the electrodeposited Zn layer and Cu foil, reducing interface resistance and solving the problem of cycling stability for cells caused by the shedding of active materials during the cycle [34,35]. The elemental mapping results show a part of interfacial fusion of Zn and Cu, therein carbon origins from the GO (Fig. 2h). Further, the wettability of these substrates in ether electrolyte coincides with the battery test results[36,37]. The functional groups and defects of GO endow GO-Zn/Cu electrode with faster wettability (~0°, lowest contact angle) in GO-Zn/Cu substrate than that in Zn/Cu (13°) and Cu (35.5°) substrates (Fig. 2i). Thus, it allows better contacts between electrolytes and substrates to provide easier access for Li-ions, which is another beneficial feature of graphene as a stable interface layer on the electrode.

Li plating/stripping electrochemistry. Next, we investigated the Li plating/stripping electrochemical behavior on composited GO-Zn/Cu, Zn/Cu, pure Cu and GO/Cu substrates (Fig. 3 and Fig. S7). The curves of initial Li metal plating on different substrates at 0.2 mA cm^{-2} are shown in Fig. S8. The GO-Zn/Cu electrode shows nucleation overpotentials of 9.3 and 22.0 mV at current densities of 0.2 and 1 mA cm^{-2}, respectively, for metal Li deposition, which are the lowest compared to other electrodes (Fig. 3a). These results confirm the accelerated Li-ion transfer driven by the synergistic effect of ion conductive GO and lithiophilic Zn. Subsequently, the cyclic voltammetry (CV) (Fig. S9) and electrochemical impedance spectrum (EIS) were recorded to gain in-depth understanding of the electrochemical activity and enhanced interface dynamics [30]. Nyquist plots for different substrates after the 1st and 50th cycles are shown in Fig. S10 and Fig. 3b, respectively, with the equivalent circuit depicted in the inset of Fig. 2b. The corresponding impedance fitting data (R_s, R_{sei}, R_{ct}) for bare Cu, Zn/Cu, GO/Cu and GO-Zn/Cu substrates are shown in Table S1. After the 1st Li cycle,

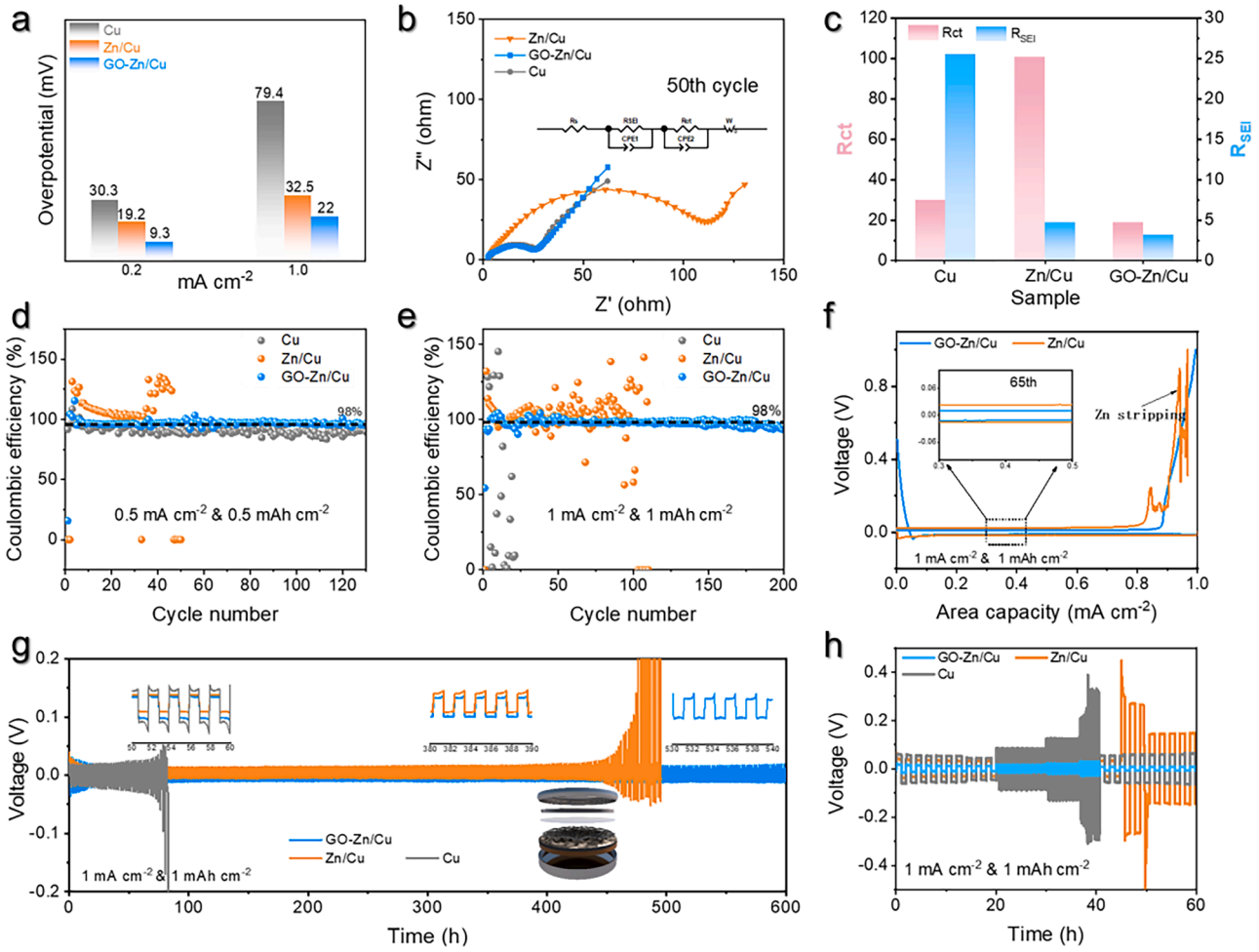

Fig. 3. Li plating/stripping behavior on composited GO-Zn/Cu, Zn/Cu and pure Cu substrates. (**a**) Comparison of nucleation overpotential of the cells. (**b**) EIS spectra and equivalent circuit fitting of half cells with different substrates as working electrode after 50th cycle. (c) The corresponding impedance fitting data (R_{sei}, R_{ct}) for bare Cu, Zn/Cu and GO-Zn/Cu substrates. (**d, e**) Coulombic efficiencies of Li plating/stripping on different substrates at current densities of (**d**) 0.5 mA cm^{-2}, (**e**) 1.0 mA cm^{-2}, and (**f**) 65th charge-discharge curves. (**g**) Comparison of the cycling stability of symmetric cells with Li@Cu, Li@Zn/Cu, and Li@GO-Zn/Cu electrodes with a current density of 1 mA cm^{-2} and (**h**) the voltage evolution of symmetrical cells at various current densities.

GO/Cu and GO-Zn/Cu exhibit larger charge transfer resistance (R_{ct}) and Li^+ migration impedance in the interphase (R_{sei}) compared to that of Cu and Zn/Cu substrates, probably due to the low conductivity of GO before activation. After 50 cycles, the R_{sei} and R_{ct} of GO-modified electrode (GO-Zn/Cu, GO/Cu) decrease significantly, and the GO-Zn/Cu substrate exhibits the lowest total interface impedance ($R_{sei} + R_{ct}$), illustrating the synergistic effect in optimizing the comprehensive interface kinetics (Fig. 3c).

Furthermore, we evaluated the coulombic efficiency (CE) and cycling stability of different Li metal anodes. As presented in Fig. 3d, the CE test was conducted at a current density of 0.5 mA cm^{-2} and a fixed capacity of 0.5 mAh cm^{-2}. The average CE of Li plating/stripping in GO-Zn/Cu||Li cell is approximately 98% for 130 cycles. In contrast, the average CEs of Cu||Li, GO/Cu||Li and Zn/Cu||Li cells decrease below 90% after 23, 38, and 46 cycles, respectively. When the cycling capacity limitation and current density increase to 1.0 mAh cm^{-2} and 1.0 mA cm^{-2}, the average CE of the GO-Zn/Cu||Li cell can still be preserved at approximately 98% for 200 cycles (Fig. 3e). Furthermore, even under deep Li plating/stripping (2-4 mAh cm^{-2}) at a large current density (1-2 mA cm^{-2}), GO-Zn/Cu presents an average CE of 96% and 88.1%, corresponding stable charge-discharge profiles within 110 and 90 cycles (Fig. S11), which also outperforms the other substrates. All these results demonstrate the significant improvement in cycling stability of the GO-Zn/Cu composite electrode compared to other types of electrodes.

Notably, as presented in Fig. 3d and e, the CE of the Zn/Cu cell is greater than 100% during initial several cycles and then rapidly decreases, while the GO-Zn/Cu electrode maintains long-term stability after the a few cycles of activation. Meanwhile, the plating/stripping curves of different anodes are displayed in Fig. 3f. It can be clearly seen that a violent oscillation process occurs in the Zn/Cu anode during the charging process, suggesting that the Zn nucleation site may be unstable and undergo a stripping process together with Li. The Inductively Coupled Plasma mass spectrometry (ICP-MS) test of electrolyte (Fig. S12) further verifies that, after initial several cycles, more Zn^{2+} cations can be detected in Zn/Cu electrode (0.306 mg L^{-1}) than that in GO-Zn/Cu electrode (0.149 mg L^{-1}), indicating that graphene effectively

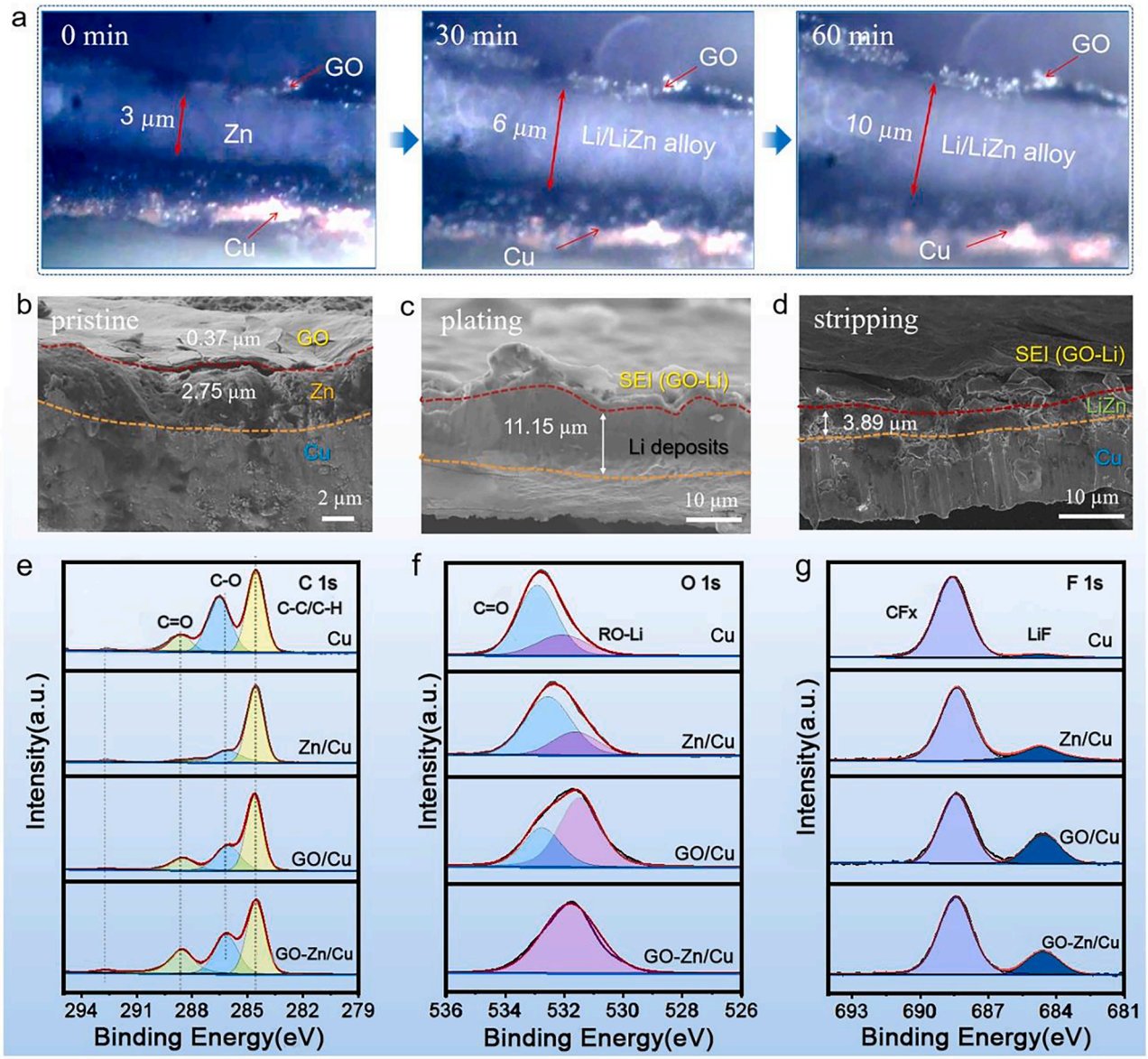

Fig. 4. (**a**) In situ optical microscopy of Li deposition at 1 mA cm^{-2}. (**b-d**) Cross-sectional SEM images of the GO-Zn/Cu electrodes: (**b**) pristine, **(c)** after the electrodeposition of 1 mAh cm^{-2} and **(d)** after the electro-stripping of 1 mAh cm^{-2}. (**e**) C 1s, (**f**) O 1s, (**g**) F 1s XPS spectra of Cu, GO/Cu, Zn/Gu, and GO-Zn/Cu substrates after several cycles.

prevents the dissolution of Zn as a seed for nucleation of LiZn alloys. This is consistent with the DFT calculation result that verifies the role of GO as interfacial layer of Li metal anode in protecting active sites and enhancing cycling stability.

Additionally, we assembled symmetry batteries with Li@Cu, Li@GO/Cu, Li@Zn/Cu and Li@GO-Zn/Cu electrodes to analyze the overpotential of Li plating/stripping. The voltage hysteresis of Li plating/stripping at 1 mA cm^{-2}/1 mAh cm^{-2} in Li@GO-Zn/Cu symmetry battery is 20 mV, smaller than that of Li@Cu (36 mV), Li@GO/Cu (34 mV), Li@Zn/Cu (24 mV). And they can be cycled for 620, 75, 180 and 460 h, respectively (Fig. 3g). Furthermore, the rate capability of the Li@GO-Zn/Cu||Li@GO-Zn/Cu symmetry cell was cycled at current densities of 1, 2, 3, 5 and 1 mA cm^2 for 20 cycles. Fig. 3h presents that the symmetrical cell performs perfect cycle stability, especially consistently displaying low overpotential fluctuations even if the current density is switched back from 5 to 1 mA cm^{-2}. The results prove that the integrated multifunctional composite structure can effectively stabilize the Li metal anode.

Structural evolution during Li plating/stripping. The structural evolution of GO-Zn/Cu anode before and after cycles was further elucidated by in situ optical microscope, ex-situ SEM and X-ray photoelectron spectroscopy (XPS). Fig. 4a shows the in situ optical microscopy of Li deposition. It can be observed that the thickness of the intermediate Zn layer under GO interface continues to increase from 3 to 10 μm due to Li preferential deposition with deposition time (0, 30 and 60 min) (Movie S1). Further results can be found from ex-situ SEM images in Fig. 4b-d. Fig. 4b shows the GO and Zn layers in the pristine GO-Zn/Cu electrode with thickness of 0.37 and 2.75 μm, respectively. After depositing Li at 1 mA cm^{-2} for 1 h, the thickness of Zn layer increases to 11.15 μm (Fig. 4c), corresponding to a 3.05 times expansion. Then Li was stripped from the Li/LiZn phase, while the LiZn alloy remained on the substrate, which are verified by XRD analysis (Fig. S13). More importantly, the GO-Zn/Cu electrode structure remains intact due to the protection of the uniform SEI (GO-Li) during stripping (Fig. 4d), and the smooth surface feature of GO-Zn/Cu electrode shows in Fig. S14 after 1 st stripping. in contrast, the surface of Zn/Cu without GO coating becomes rough and porous (Fig. S15), which would cause uneven Li deposition and induce Li dendrite growth. These results suggest that the electrodeposited Li on GO-Zn/Cu electrode is mainly stored beneath the GO layer in Li metal anode, while the GO is stable and can maintain the sustainability of the active site as an interface.

Furthermore, high-resolution XPS spectra were carried out to analyze the chemical surface composition of the four electrodes (Fig. 4e-g). The C=O peak is attributed to Li_2CO_3 of Cu substrate (289.8 eV in C 1s) [38], while the C=O peak is assigned to the GO phase in GO/Cu and GO-Zn/Cu surfaces (289.7 eV in C 1s) [39] (Fig. 4e). Higher RO-Li peak (531.7 eV in O 1s) [40,41] is displayed in both GO-contained substrates. In particular, the GO-Zn/Cu electrode surface is completely occupied by inorganic materials (Fig. 4f), which manifests stable chemical-bond generated between Li and GO in ether-based electrolyte, consistent with previous DFT calculation results. And RO-Li with a low oxidation state is an essential component for the construction of a stable SEI [42]. Except for Cu substrate, the F 1s peak at 684.44 eV is seen in Zn/Cu, GO/Cu and GO-Zn/Cu substrates, respectively, which is assigned to LiF [43] (Fig. 4g), implying that either GO or Zn modification can easily enriches SEI with LiF components. While the surface of electrode is covered with flat graphene (GO/Cu and GO-Zn/Cu), the native SEI with the higher LiF content is formed. In general, due to the coexistence of graphene and zinc, the surface of GO-Zn/Cu produces favorable Li^+ conductive LiF and stable RO-Li, as same as the EIS test result, which improves the interface kinetics and stability [30,42,44-48]. Furthermore, the evidences from XPS further suggest that Li metal is deposited underneath the GO layer, consistent with the above observation results from SEM and in-situ optical microscopy. The dense native SEI layer is formed on the surface of GO by the decomposition of the ether-base electrolyte during cycling and preserves integrity, which steadily accelerates ionic transfer.

To further probe the role of the sandwich structure on Li plating/stripping behaviors, we investigated the surface structure of electrodes in different states with different cycles. It can be seen from Fig. 5a that, after the 1st plating process, some large lumps of Li are formed on Cu substrate. In contrast, Fig. 5b and c show that both GO and Zn metal have the ability to induce Li deposition, which can be attributed to the effect of the GO interfacial layer in homogenizing the Li ion flow [37,49] and the fact that Zn metal would form a lithiophilic alloy with deposited Li [20]. Naturally, Li deposition underneath the GO layer has a more homogeneous structure in GO-Zn/Cu composite electrodes (Fig. 5d). Fig. 5e-f show the surface morphology of the Cu, GO/Cu, Zn/Cu and GO-Zn/Cu electrodes after the 1st Li-stripping. For pure Cu electrode (Fig. 5e), a large number of cavities are present on the electrode, with very rough appearance. Meanwhile, a small number of dendrites occur on GO/Cu electrode (Fig. 5f), and some nano-metals separated by SEI are visible on Zn/Cu electrode (Fig. 5g). Obviously, Zn NPs only exist in the composite electrode, which are still uniformly attached under the graphene interface layer (Fig. 5h). This means that either the artificial SEI design or the pro-lithium layer modification would not sufficient for suppression of dendrites and "dead" Li, while their synergistic effect is required.

Furthermore, after 50 stripping cycles, an in-depth comparative analysis of the surface structure of the four electrodes was conducted. A large amount of massive “dead” Li accumulation can be found on Cu and GO/Cu substrates (Fig. 5i-j), which illustrate the poor cycling stability of such half cells. For Zn/Cu substrate, deformation can be found after stripping, ascribed to the stable line compounds formed during the Li redirection induced by the introduction of Zn, which finally results in uneven Li deposition and dendrite growth near the voids and cracks of Zn layers after 50 cycles (Fig. 5k). The above ICP-MS analysis (Fig. S12) of the electrolyte confirms that the formation of these voids can be caused by the partial dissolution of the Zn metal seeds. In contrast, the smooth and flat surface of the GO-Zn/Cu composite electrode appears after 50 cycles, and no Li dendrites can be observed at all (Fig. 5i). Based on these results, we propose a synergistic effect that enables the complete suppression of dendrite and "dead" Li on GO-Zn/Cu substrate.

Performance of full pouch cell. We further evaluated the practical application scenarios of GO-Zn/Cu electrode. The full cells coupled Li@Cu, Li@GO/Cu, Li@Zn/Cu and Li@GO-Zn/Cu (metal Li 10 mAh cm^{-2}) anodes with commercial LFP (11.5 mg cm^{-2}) cathodes were assembled, which reached a practically low N/P ratio of 5:1 (Fig. 6a). First, the corresponding pouch cells were assembled to confirm the practicality and the feasibility. After charging to 4.0 V, the flexible cell can stably power the light-emitting diode, which needs 2.9~3.2 V to light up, regardless of large-angle bending and distorting (Fig. 6b and c). This demonstrates the superior conductivity and excellent mechanical stability, which promise its applications in flexible electronics.

Next, we probed the multiplier performance of these full cells. Fig. 6d shows the typical discharge-charge profiles of LFP||Li@GO-Zn/Cu. Its voltage platform does not much fluctuate with different current densities, and still keeps higher specific capacity and small polarization voltage relative to the others even at 5 C. Although all full cells exhibit a similar capacity at low rates (160 mAh g^{-1} at 0.1 C) (Fig. 6e), a higher areal capacity at high rates (such as 80 mAh g^{-1} at 5 C, capacity retention 49.3%) is achieved for LFP||Li@GO-Zn/Cu full cells compared with others. Moreover, when the current density changes back to 0.1 C, the reversible capacity of LFP||Li@GO-Zn/Cu can be fully recovered, indicating stable reversibility of the thus-formed full cells. Then the polarization voltage (ΔV) was calculated from difference charging/discharging platforms. As presented in Fig. 6f, compared with other electrodes, no matter how different the current density, LFP||Li@GO-Zn/Cu still maintains the minimum ΔV value. Especially, the ΔV value of LFP||Li@GO-Zn/Cu is 0.305 V at the high current density of 5 C, less than LFP||Li@Cu cell (0.755 V), LFP|| Li@GO/Cu (0.578 V), and LFP|| Li@Zn/Cu (0.467 V). The higher rate capability and lower polarization

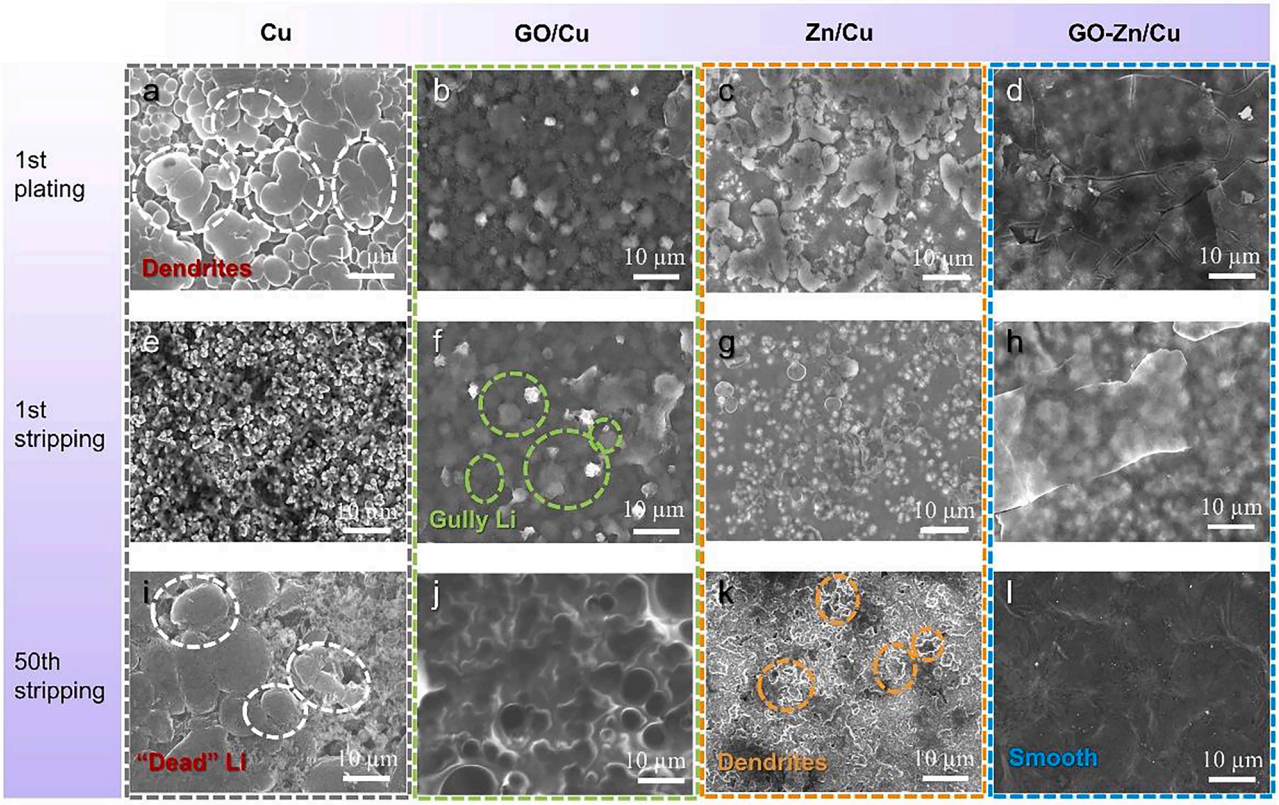

Fig. 5. SEM images of (**a, e, i**) Cu, (**b, f, j**) GO/Cu, (**c, g, k**) Zn/Cu, and (**d, h, l**) GO-Zn/Cu substrates after 1st Li plating/ stripping and 50th stripping cycles at 1 mA cm^{-2} with a capacity of 1.0 mAh cm^{-2}.

at high rates can be attributed to the fast ion transfer of GO and sustainability of lithiophilic Zn layers.

Furthermore, long-term cycling performance demonstrates that, after only 10 cycles at 1 C, bare LFP||Li@Cu shows rapid capacity decay, and only negligible capacity could be retained after 50 cycles, mainly attributed to the inhomogeneity and roughness of the bare Cu electrode surface, in accompany with the lithiophobic properties that may result in the severe formation of Li dendrites and "dead" Li on the surface of Li metal anode with obvious cracks. In sharp contrast, LFP||Li@GO-Zn/Cu exhibits a highly stable cycling performance over 100 cycles with a capacity retention of 81.1%, compared with bare Cu (0%), GO/Cu (47.6%) and Zn/Cu (40.6%) (Fig. 6g). Specifically, from the 62th charge/discharge curves of LMBs at 1 C in Fig. S16, the LFP||Li@GO-Zn/Cu full cell delivers the highest specific capacity (138 mAh g^{-1}) and the lowest voltage polarization among full cells. As seen from the electrochemical performance of different host materials listed in Table S2, this work plays an positive role with commercial applications. Therefore, it can be concluded that the cells prepared with modified Cu anodes (LFP||Li@GO-Zn/Cu) possess improved capacity retention owing to steady work of lithiophilic Zn which can serve as nucleation seeds to facilitate the uniformity of the initial nucleation behavior. Consequently, the GO with ion selectivity, as an artificial protective layer, effectively anchors the Zn^{2+} from dealloying to keep the Zn layer sustainable after stripping, and the GO with high Li ion conductivity component results in fast and uniform Li deposition.

3. Conclusion

In conclusion, we have systematically investigated the role of graphene oxide (GO) in stabilizing nucleation Zn seeds during the Li stripping and plating process by building a unique sandwich structured lithium (Li) metal anode. Owing to strong Zn adsorption effect and high Li ion conductivity of GO as an artificial SEI layer, it effectively blocks Zn transport from the alloy to the electrolyte and boosts Li diffusion kinetics from GO surfaces to Zn layers toward favorable Li plating into Zn seeds. Therefore ion-selective graphene is capable of maintaining the lithiophilic Zn stability, which synergistically stabilizing the reversible Zn during the Li stripping process. Coupled with the important role of graphene interphase in strong mechanical properties to overcome large volume change during the Li stripping and plating process, the GO-Zn/Cu||Li half-cell exhibits stable cycling performance with a high average CE of ~98%, and the LFP||Li@GO-Zn/Cu full cell with high mass loading (11.5 mAh g^{-1}) shows high capacity retention (~87%) after 100 cycles. The combination of the lithiophilic Zn and GO coating not only preserves uniform Li plating but also maintain stability of nucleation sites. This work describes a discovery that Zn^{2+} is easy to enter the electrolyte from the alloy during Li stripping and affects the stability of nucleation seeds. Therefore, ion-selective graphene can maintain metal site sustainability and improve cycling performance of the battery.

4. Experimental section

4.1. Material synthesis

Preparation of Zn/Cu substrate: Zn was directly deposited on Cu foil by an electrodeposition method, employing a CHI 660E workstation. In brief, a piece of Cu foil was used as work electrode (2 cm × 2 cm) and precleaned by ethyl alcohol cotton ball. 6.25 g zinc sulfate ($ZnSO_4{\cdot}7H_2O$), 6.25 g sodium sulfate (Na_2SO_4), and 1 g boric acid (H_3BO_3) was dissolved in 50 mL distilled water and used as electrolyte. The electrodeposition was conducted with a constant current density of -16 mA cm^{-2} for 450 s at room temperature. The mass loading of the Zn cathode is 6.14 mg cm^{-2}, which was obtained by electronic scales (BT25S, 0.01 mg).

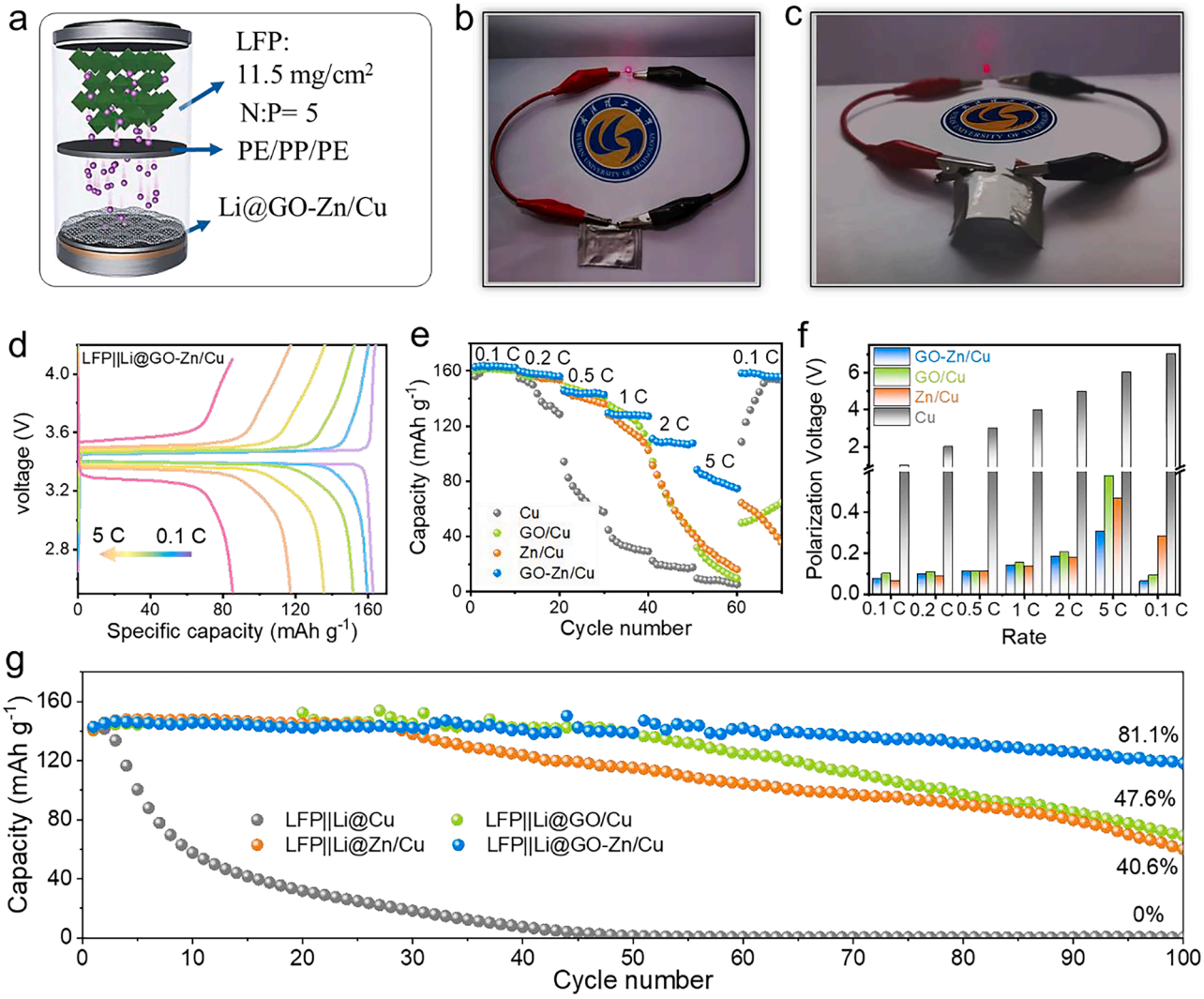

Fig. 6. (**a**) Schematic diagram of LFP||Li@GO-Zn/Cu full cells. (**b, c**) Photographs of the original (**b**) and bent (**c**) flexible pouch full-cell powering a light-emitting diode board. (**d**) The charge/discharge voltage-capacity profiles of LFP||Li@GO-Zn/Cu full cells at various current densities. (**e**) Rate performance and (**f**) the corresponding polarization voltage of the LFP//Li@Cu, LFP//Li@GO/Cu, LFP//Li@Zn/Cu and LFP//Li@GO-Zn/Cu cells at 0.1, 0.2, 0.5, 1, 2 and 5 C. (**g**) Cycling perfoemance of the four types of full cells at 1 C.

Preparation of GO-Zn@Cu substrate: Graphene was uniformly dispersed in DI at 1 mg mL^{-1}. Take a small amount of the dispersion with a dropper and spin-coat it onto the Zn/Cu substrate several times. Finally, the GO-Zn/Cu substrate covered with GO is obtained until the solvent is evaporated.

4.2. Electrochemical tests

All cells were assembled with CR2023 coins. Symmetrical cells were equipped with two Li foils (radius of 16 mm) as working electrodes and a separator. Half cells used Li foil and Cu, GO/Cu, Zn/Cu, GO-Zn/Cu substrate (radius of 16 mm) as working electrodes coupled with a separator. 40 μL of LiTFSI (1 M) electrolyte in a mixed solvent of DOL and DME (1:1 v/v) with 1 wt % $LiNO_3$ additives was used in symmetrical cells and half cells. In full cells, the cathode electrode of a commercial 11.5 mg cm^{-2} LFP active material, and coupled with pre-position 10 mAh cm^{-2} Li (Li@Cu, Li@GO/Cu, Li@Zn/Cu, Li@GO-Zn/Cu anode). The Neware battery test systems were served for electrochemical measurements after resting for 12 h and activating. The activation procedures of half-cell tests were based on a discharge/charge voltage window of 0.01-0.2 V, and in subsequent cycles, the discharge time was controlled and the charge cutoff voltage of 0.2 V was adopted. The symmetric cells and full cells are activated at 0.25 mA cm^{-2} for five cycles and at 0.2 C (1 C = 170 mA g^{-1}) in the initial two cycles, respectively. An Autolab electrochemical workstation (NOVA 1.9) was used for the EIS with a frequency ranging from 100 Hz to 0.01 Hz and a perturbation amplitude of 5 mV.

4.3. Material characterizations

The morphology analysis was executed by SEM (SU-70), and the crystalline structures were demonstrated by XRD (Ultima IV) with Cu Kα radiation. Compositional analysis was carried out by X-ray photoelectron spectrometry (XPS, Thermo Scientific ESCALAB Xi^+). For XRD measurement after cycled samples, polyimide tape was used to encapsulate them in a vacuum condition. The Li||GO-Zn/Cu cell (LIB-MS-II; Beijing Science Star technology Co. Ltd.) was monitored in situ visually with an optical microscope (SZ900) during Li deposition.

4.4. First-principles calculation

Density functional theory (DFT) calculations in this work were carried out using the CASTEP program on Materials Studio. A supercell model is employed to simulate the graphene, The exchange-correlation effects were described by the Perdew-Burke-Ernzerhof (PBE) functional

within the generalized gradient approximation (GGA) method. The core-valence interactions were accounted by the projected augmented wave (PAW) method [28,29]. The energy cutoff for plane wave expansions wasset to 400 eV, and the 3×3×1 Monkhorst-Pack grid k-points were selected to sample the Brillouin zone integration. The vacuum space is adopted 20 Å above the surfaces to avoid periodic interactions. The structural optimization was completed for energy and force convergence set at 1.0×10^{-5} eV and 0.03 eV $Å^{-1}$, respectively. Each model was allowed to interact with a Li ion and the binding energy is defined as Eq. (1):

$$E_b = E_{total} - E_{sub} - E_{ion} \quad (1)$$

where E_{total}, E_{sub}, and E_{ion} are the energy of GO model bound with Li^+/Zn^{2+}, GO model, and Li^+/Zn^{2+}, respectively.

CRediT authorship contribution statement

The manuscript was written through contributions of all authors. All authors have given approval to the final version of the manuscript. **Jingjing Ma** and **Jinglong Yang**: contributed equally on sample synthesis, data acquisition and analysis, Writing-original draft and manuscript preparation. **Meng Huang** and **Jiawei Zhu**: DFT calculations, data analysis, Supervision, **Weihao Zeng** and **Xin Zhao**: manuscript preparation. **Lun Li, Peng Li Fan Qiao** and **Zixin Zhang**: Experimental test, data analysis and Diagram arrangement. **Daping He**: Resources, Supervision, Funding acquisition, Writing – review & editing. **Shichun Mu**: Conceptualization, Investigation, Methodology, Formal analysis, Resources, Supervision, Funding acquisition, Writing – review & editing.

Supporting Information

Supporting Information is available from the Wiley Online Library or from the author.

Declaration of Competing Interest

The authors declare that they have no known competing financial interests or personal relationships that could have appeared to influence the work reported in this paper.

Acknowledgement

This work was financially supported by the National Key Research and Development Program of China (No. 2016YFA0202603), the National Natural Science Foundation of China (52172217), Natural Science Foundation of Guangdong Province (2021A1515010144), and Shenzhen Science and Technology Program (JCYJ20210324120400002), the State Key Laboratory of Advanced Technology for Materials Synthesis and Processing (Wuhan University of Technology) (2022-ZD-4).

Supplementary materials

Supplementary material associated with this article can be found, in the online version, at doi:10.1016/j.ensm.2023.01.045.

References

[1] X.B. Cheng, R. Zhang, C.Z. Zhao, Q. Zhang, Toward Safe Lithium Metal Anode in Rechargeable Batteries: A Review, Chem. Rev 117 (2017) 10403–10473.
[2] B. Li, Y. Wang, S. Yang, A material perspective of rechargeable metallic lithium anodes, Adv. Energy Mater. 8 (2018), 1702296.
[3] D. Lin, Y. Liu, Y. Cui, Reviving the lithium metal anode for high-energy batteries, Nat. nanotechnol. 12 (2017) 194–206.
[4] F. Ding, W. Xu, G.L. Graff, J. Zhang, M.L. Sushko, X. Chen, Y. Shao, M. H. Engelhard, Z. Nie, J. Xiao, X. Liu, P.V. Sushko, J. Liu, J.-G. Zhang, Dendrite-Free Lithium Deposition via Self-Healing Electrostatic Shield Mechanism, Journal of the J. Am. Chem. Soc 135 (2013) 4450–4456.
[5] R. Bhattacharyya, B. Key, H. Chen, A.S. Best, A.F. Hollenkamp, C.P. Grey, In situ NMR observation of the formation of metallic lithium microstructures in lithium batteries, Nat. Mater 9 (2010) 504–510.
[6] D. Lu, Y. Shao, T. Lozano, W.D. Bennett, G.L. Graff, B. Polzin, J. Zhang, M. H. Engelhard, N.T. Saenz, W.A. Henderson, Failure mechanism for fast-charged lithium metal batteries with liquid electrolytes, Adv. Energy Mater. 5 (2015), 1400993.
[7] Y.X. Zhan, P. Shi, R. Zhang, X.Q. Zhang, X. Shen, C.B. Jin, B.Q. Li, J.Q. Huang, Deciphering the effect of electrical conductivity of hosts on lithium deposition in composite lithium metal anodes, Adv. Energy Mater. 11 (2021), 2101654.
[8] Y.X. Zhan, P. Shi, C.B. Jin, Y. Xiao, M.Y. Zhou, C.X. Bi, B.Q. Li, X.Q. Zhang, J. Q. Huang, Regulating the Two-Stage Accumulation Mechanism of Inactive Lithium for Practical Composite Lithium Metal Anodes, Adv. Funct. Mater 32 (2022), 2206834.
[9] P. Shi, Z.-Y. Liu, X.-Q. Zhang, X. Chen, N. Yao, J. Xie, C.-B. Jin, Y.-X. Zhan, G. Ye, J.-Q. Huang, Polar interaction of polymer host–solvent enables stable solid electrolyte interphase in composite lithium metal anodes, J. Energy Chem. 64 (2022) 172–178.
[10] R. Zhang, X.R. Chen, X. Chen, X.B. Cheng, X.Q. Zhang, C. Yan, Q. Zhang, Lithiophilic sites in doped graphene guide uniform lithium nucleation for dendrite-free lithium metal anodes, Angew. Chem. 129 (2017) 7872–7876.
[11] N.W. Li, Y.X. Yin, C.P. Yang, Y.G. Guo, An Artificial Solid Electrolyte Interphase Layer for Stable Lithium Metal Anodes, Adv. Mater. 28 (2016) 1853–1858.
[12] J. Wu, Z. Rao, X. Liu, Y. Shen, L. Yuan, Z. Li, X. Xie, Y. Huang, Composite lithium metal anodes with lithiophilic and low-tortuosity scaffold enabling ultrahigh currents and capacities in carbonate electrolytes, Adv. Funct. Mater 31 (2021), 2009961.
[13] S.S. Zhang, X. Fan, C. Wang, A tin-plated copper substrate for efficient cycling of lithium metal in an anode-free rechargeable lithium battery, Electrochim. Acta 258 (2017) 1201–1207.
[14] R. Song, Y. Ge, B. Wang, Q. Lv, F. Wang, T. Ruan, D. Wang, S. Dou, H. Liu, A new reflowing strategy based on lithiophilic substrates towards smooth and stable lithium metal anodes, J. Mater. Chem. A 7 (2019) 18126–18134.
[15] K. Yan, Z. Lu, H.-W. Lee, F. Xiong, P.-C. Hsu, Y. Li, J. Zhao, S. Chu, Y. Cui, Selective deposition and stable encapsulation of lithium through heterogeneous seeded growth, Nat. Energy 1 (2016) 1–8.
[16] H. Wang, Y. Li, Y. Li, Y. Liu, D. Lin, C. Zhu, G. Chen, A. Yang, K. Yan, H. Chen, Wrinkled graphene cages as hosts for high-capacity Li metal anodes shown by cryogenic electron microscopy, Nano lett 19 (2019) 1326–1335.
[17] H. Fan, C. Gao, Q. DonG, B. Hong, Z. FanG, M. Hu, Y. Lai, Silver sites guide spatially homogeneous plating of lithium metal in 3D host, J. electroanal. chem. 824 (2018) 175–180.
[18] Q. Sun, W. Zhai, G. Hou, J. Feng, L. Zhang, P. Si, S. Guo, L. Ci, In situ synthesis of a lithiophilic Ag-nanoparticles-decorated 3D porous carbon framework toward dendrite-free lithium metal anodes, ACS Sustain. Chem. Eng. 6 (2018) 15219–15227.
[19] T. Liu, J. Zheng, H. Hu, O. Sheng, Z. Ju, G. Lu, Y. Liu, J. Nai, Y. Wang, W. Zhang, In-situ construction of a Mg-modified interface to guide uniform lithium deposition for stable all-solid-state batteries, J. Energy Chem. 55 (2021) 272–278.
[20] K. Xu, M. Zhu, X. Wu, J. Liang, Y. Liu, T. Zhang, Y. Zhu, Y. Qian, Dendrite-tamed deposition kinetics using single-atom Zn sites for Li metal anode, Energy Stor. Mater. 23 (2019) 587–593.
[21] C. Wang, Y. Gong, B. Liu, K. Fu, Y. Yao, E. Hitz, Y. Li, J. Dai, S. Xu, W. Luo, Conformal, nanoscale ZnO surface modification of garnet-based solid-state electrolyte for lithium metal anodes, Nano lett 17 (2017) 565–571.
[22] Y. Xu, S. Zhao, G. Zhou, W. Chen, F. Zhou, Z. Rong, Y. Wu, J. Li, J. Guo, Y. Zhang, Solubility-dependent protective effects of binary alloys for lithium anode, ACS Appl. Energy Mater. 3 (2020) 2278–2284.
[23] Y.X. Zhan, P. Shi, X.X. Ma, C.B. Jin, Q.K. Zhang, S.J. Yang, B.Q. Li, X.Q. Zhang, J. Q. Huang, Failure mechanism of lithiophilic sites in composite lithium metal anode under practical conditions, Adv. Energy Mater. 12 (2022), 2103291.
[24] C. Yang, Y. Yao, S. He, H. Xie, E. Hitz, L. Hu, Ultrafine silver nanoparticles for seeded lithium deposition toward stable lithium metal anode, Adv. Mater. 29 (2017), 1702714.
[25] J. Meng, Q. He, L. Xu, X. Zhang, F. Liu, X. Wang, Q. Li, X. Xu, G. Zhang, C. Niu, Identification of phase control of carbon-confined Nb2O5 nanoparticles toward high-performance lithium storage, Adv. Energy Mater. 9 (2019), 1802695.
[26] G. Jiang, N. Jiang, N. Zheng, X. Chen, J. Mao, G. Ding, Y. Li, F. Sun, Y. Li, MOF-derived porous Co3O4-NC nanoflake arrays on carbon fiber cloth as stable hosts for dendrite-free Li metal anodes, Energy Stor. Mater. 23 (2019) 181–189.
[27] H. Tian, Z.W. Seh, K. Yan, Z. Fu, P. Tang, Y. Lu, R. Zhang, D. Legut, Y. Cui, Q. Zhang, Theoretical Investigation of 2D Layered Materials as Protective Films for Lithium and Sodium Metal Anodes, Adv. Energy Mater. 7 (2017).
[28] G. Li, S. Zhou, J. Zhao, First-Principles Study of Lithium Adsorption, Storage and Diffusion Properties for Graphite Oxides, J. Nanosci. Nanotechnol. 16 (2016) 8106–8112.
[29] L.-J. Zhou, Z.F. Hou, L.-M. Wu, Y.-F. Zhang, First-Principles Studies of Lithium Adsorption and Diffusion on Graphene with Grain Boundaries, J. Phys. Chem. C 118 (2014) 28055–28062.
[30] L. Lin, F. Liu, Y. Zhang, C. Ke, H. Zheng, F. Ye, X. Yan, J. Lin, B. Sa, L. Wang, D. L. Peng, Q. Xie, Adjustable Mixed Conductive Interphase for Dendrite-Free Lithium Metal Batteries, ACS Nano (2022).
[31] S.C. O'Hern, M.S. Boutilier, J.-C. Idrobo, Y. Song, J. Kong, T. Laoui, M. Atieh, R. Karnik, Selective ionic transport through tunable subnanometer pores in single-layer graphene membranes, Nano lett 14 (2014) 1234–1241.

[32] R. Tarcan, O. Todor-Boer, I. Petrovai, C. Leordean, S. Astilean, I. Botiz, Reduced graphene oxide today, 8 (2020) 1198-1224.
[33] K.S. Kim, Y. Zhao, H. Jang, S.Y. Lee, J.M. Kim, K.S. Kim, J.-H. Ahn, P. Kim, J.-Y. Choi, B.H. Hong, Large-scale pattern growth of graphene films for stretchable transparent electrodes, Nature 457 (2009) 706–710.
[34] C. Yang, K. Fu, Y. Zhang, E. Hitz, L. Hu, Protected lithium-metal anodes in batteries: from liquid to solid, Adv. Mater. 29 (2017), 1701169.
[35] Y. Guo, H. Li, T. Zhai, Reviving lithium-metal anodes for next-generation high-energy batteries, Adv. Mater. 29 (2017), 1700007.
[36] S. Chattopadhyay, A.L. Lipson, H.J. Karmel, J.D. Emery, T.T. Fister, P.A. Fenter, M. C. Hersam, M.J. Bedzyk, In Situ X-ray Study of the Solid Electrolyte Interphase (SEI) Formation on Graphene as a Model Li-ion Battery Anode, Chem. Mater. 24 (2012) 3038–3043.
[37] Z.T. Wondimkun, W.A. Tegegne, J. Shi-Kai, C.-J. Huang, N.A. Sahalie, M.A. Weret, J.-Y. Hsu, P.-L. Hsieh, Y.-S. Huang, S.-H. Wu, W.-N. Su, B.J. Hwang, Highly-lithiophilic Ag@PDA-GO film to Suppress Dendrite Formation on Cu Substrate in Anode-free Lithium Metal Batteries, Energy Stor. Mater. 35 (2021) 334–344.
[38] Y. Yu, Z. Yang, Y. Liu, J. Xie, Achieving SEI preformed graphite in flow cell to mitigate initial lithium loss, Carbon (2022).
[39] R. Al-Gaashani, A. Najjar, Y. Zakaria, S. Mansour, M.A. Atieh, XPS and structural studies of high quality graphene oxide and reduced graphene oxide prepared by different chemical oxidation methods, Ceram. int. 45 (2019) 14439–14448.
[40] Z. Hou, J. Zhang, W. Wang, Q. Chen, B. Li, C. Li, Towards high-performance lithium metal anodes via the modification of solid electrolyte interphases, J. Energy Chem. 45 (2020) 7–17.
[41] Z. Dai, H. Zhao, W. Chen, Q. Zhang, X. Song, G. He, Y. Zhao, X. Lu, Y. Bai, In Situ Construction of Gradient Oxygen Release Buffer and Interface Cation Self-Accelerator Stabilizing High-Voltage Ni-Rich Cathode, Adv. Funct. Mater (2022), 2206428.
[42] K. Yan, J. Wang, S. Zhao, D. Zhou, B. Sun, Y. Cui, G. Wang, Temperature-dependent Nucleation and Growth of Dendrite-free Lithium Metal Anodes, Angew. Chem. 131 (2019) 11486–11490.
[43] X.Q. Zhang, X. Chen, X.B. Cheng, B.Q. Li, X. Shen, C. Yan, J.Q. Huang, Q. Zhang, Highly stable lithium metal batteries enabled by regulating the solvation of lithium ions in nonaqueous electrolytes, Angew. Chem. International Edition 57 (2018) 5301–5305.
[44] R. Xu, Y. Xiao, R. Zhang, X.B. Cheng, C.Z. Zhao, X.Q. Zhang, C. Yan, Q. Zhang, J. Q. Huang, Dual-phase single-ion pathway interfaces for robust lithium metal in working batteries, Adv. Mater. 31 (2019), 1808392.
[45] K. Yan, B. Sun, P. Munroe, G. Wang, Three-dimensional pie-like current collectors for dendrite-free lithium metal anodes, Energy Stor. Mater. 11 (2018) 127–133.
[46] M. Chen, J. Zheng, Y. Liu, O. Sheng, Z. Ju, G. Lu, T. Liu, Y. Wang, J. Nai, Q. Wang, Marrying ester group with lithium salt: Cellulose-acetate-enabled LiF-enriched interface for stable lithium metal anodes, Adv. Funct. Mater 31 (2021), 2102228.
[47] Y.H. Tan, G.X. Lu, J.H. Zheng, F. Zhou, M. Chen, T. Ma, L.L. Lu, Y.H. Song, Y. Guan, J. Wang, Lithium Fluoride in Electrolyte for Stable and Safe Lithium-Metal Batteries, Adv. Mater. 33 (2021), 2102134.
[48] O. Sheng, J. Zheng, Z. Ju, C. Jin, Y. Wang, M. Chen, J. Nai, T. Liu, W. Zhang, Y. Liu, In situ construction of a LiF-enriched interface for stable all-solid-state batteries and its origin revealed by cryo-TEM, Adv. Mater. 32 (2020), 2000223.
[49] M.R. Karim, K. Hatakeyama, T. Matsui, H. Takehira, T. Taniguchi, M. Koinuma, Y. Matsumoto, T. Akutagawa, T. Nakamura, S.-i. Noro, Graphene oxide nanosheet with high proton conductivity, Journal of the J. Am. Chem. Soc 135 (2013) 8097–8100.